



Effect of TiAl_3 Content on Thermal Shock Resistance of Bionic Self-healing Thermal Barrier Coatings

Panpan Zhang^{1,2} · Yujia Guo^{1,2} · Zhihui Zhang³ · Xiaofeng Zhang⁴ · Qunli Zhang^{1,2} · Jianhua Yao^{1,2}

Received: 9 August 2021 / Revised: 7 October 2021 / Accepted: 10 October 2021 / Published online: 18 November 2021
© Jilin University 2021

Abstract

Inspired by the self-healing function of biological organisms, Bionic Laser Alloying (BLA) process was adopted to fabricate the bionic self-healing Thermal Barrier Coatings (TBCs). The BLA with different fractions of TiAl_3 self-healing agent and Ceria and Yttria-Stabilized Zirconia (CYSZ) on the plasma-sprayed 7YSZ TBCs was carried out by a pulsed Nd: YAG laser. The effect of TiAl_3 content on the microstructure, phase composition, and thermal shock behaviors of the bionic self-healing TBCs were investigated. Results indicated that the bionic self-healing TBCs had better thermal shock resistance than that of the as-sprayed TBCs. The thermal shock resistance increased first and then decreased with increasing TiAl_3 fraction. The thermal shock resistance of the bionic self-healing TBCs with 15% TiAl_3 is triple that of the as-sprayed TBCs. On one hand, the columnar crystals and vertical cracks could improve strain compatibility of TBCs during the thermal shock process; on the other hand, the TiAl_3 as a self-healing agent reacted with oxygen in air at high temperature to seal the microcracks, thereby delaying the crack connection.

Keywords Thermal barrier coating · Laser · Bionic self-healing · Thermal shock resistance

1 Introduction

Thermal Barrier Coatings (TBCs) have been developed to be used as the protective coating on combustor chamber, turbine blades, and nozzle guide vanes of aircraft engines and industrial gas turbines [1–3]. The important function of the satisfactory TBCs is to provide thermal insulation to the metallic substrate, effectively reducing the operating temperature and increasing the component durability. Typically, the TBCs are multilayer systems, consisting of the Top Coating (TC), the Bond Coating (BC), and a Thermally Grown

Oxide (TGO) layer between the TC and the BC. Yttria partially Stabilized Zirconia (YSZ) is widely used as the ceramic material for the TC owing to its high melting point, low thermal conductivity, high thermal expansion coefficient, and high fracture toughness [4–6]. MCrAlY (M: Ni, Co, and Ni+Co) has been used as the BC material to protect the substrate underneath from oxidation and moderate the thermal expansion misfit between the ceramic coating and the substrate [7, 8]. The TGO layer mainly includes alumina (Al_2O_3) and some other complex oxides as $(\text{Cr}, \text{Al})_2\text{O}_3$, NiO, and $(\text{Ni}, \text{Co})(\text{Cr}, \text{Al})_2\text{O}_4$ [9, 10], which are formed because of the oxygen penetration through the ceramic coating.

The high deposition efficiency and low cost of the Air Plasma Spraying (APS) are used extensively for the deposition of ceramic coatings [11, 12]. However, the plasma-sprayed TBCs have a relatively low thermal cycling lifetime, which is governed by a sequence of crack initiation, propagation, and coalescence [13, 14]. Therefore, enhancing the crack extension resistance is an effective method for improving the thermal shock resistance of TBCs. During the process of evolution by natural selection, biological organisms [15–18] have developed their own unique structures and functions. In general, these excellent functional characteristics of biological organisms are attributed to the coupling

✉ Jianhua Yao
laser@zjut.edu.cn

¹ Institute of Laser Advanced Manufacturing, Zhejiang University of Technology, Hangzhou 310023, China

² Collaborative Innovation Center of High-End Laser Manufacturing Equipment (National “2011 Plan”), Zhejiang University of Technology, Hangzhou 310023, China

³ The Key Laboratory of Bionic Engineering (Ministry of Education China), Jilin University, Changchun 130022, China

⁴ Institute of New Materials, Guangdong Academy of Sciences, Guangzhou 510650, China

effects of morphological characteristics, internal configuration, and chemical composition. That is, some functional units, which are different from the adjacent base body in the above factors, are within the surface layer of biological organisms. These functional units are essential for comprehending the excellent properties of biomaterials. Song et al. investigated the crack evolution in nacre with sophisticated hierarchical structure under a quasi-static state and summarized that the crack deflection was favorable for enhancing the crack extension resistance [19]. Zhang et al. conducted the in situ tensile tests to explore the effect of veins on arresting cracking in the dragonfly wing and found that rigid veins could impede crack propagation [20]. Wu et al. observed the crack propagation path of plant leaf and found the crack deflection from one direction to another in plant leaf due to being blocked by the veins [21]. Consequently, those functional units exhibited excellent crack resistance by prolonging the crack propagation path and time [19–21]. Inspired by the natural phenomena, these functional units can be copied or fabricated on the artificial production to achieve some unique performances.

Bionic laser surface treatment, which combines the laser processing technology and the coupled bionic theory, is an alternative approach to fabricate the functional units. In our previous studies, the Bionic Laser Remelting (BLR) was adopted to form the functional units on the TBCs and investigated the effects of unit shape on the thermal shock resistance of TBCs [22]. And results indicated that the thermal shock resistance of the BLR specimen with dotted units was better than that of the as-sprayed specimen. Furthermore, we investigated the influence of unit distance on the thermal shock behavior and found that the BLR specimen with unit distance of 3 mm showed the best thermal shock resistance [23]. Even though the columnar grains and segmented cracks in the bionic unit allowed better strain tolerance under thermal cycles, the connection between vertical cracks and transverse cracks finally led to the spallation failure of coatings in the BLR specimen [22, 23]. It can be said that the postponed connection between vertical cracks and transverse cracks might make a new breakthrough to improve the thermal shock resistance of TBCs.

In nature, once the insect is subjected to skin damage, the exposed hemolymph will lead to the cuticular melanization (i.e., solidification) at the air/liquid interface, and finally, the insect wound will heal [24]. When the interior material of the fruit is exposed to air, the fruit surface will cause spontaneous browning by oxidation of phenolic compounds, as shown in Fig. 1. It is the biological healing materials in the insects and fruits that are oxidized by ambient oxygen for protection [24]. Inspired by the solidification chemistry of insect cuticle formation and fruit browning processes, self-healing materials, which are more similar to biological healing materials, might be one solution for filling and sealing the pores or cracks of

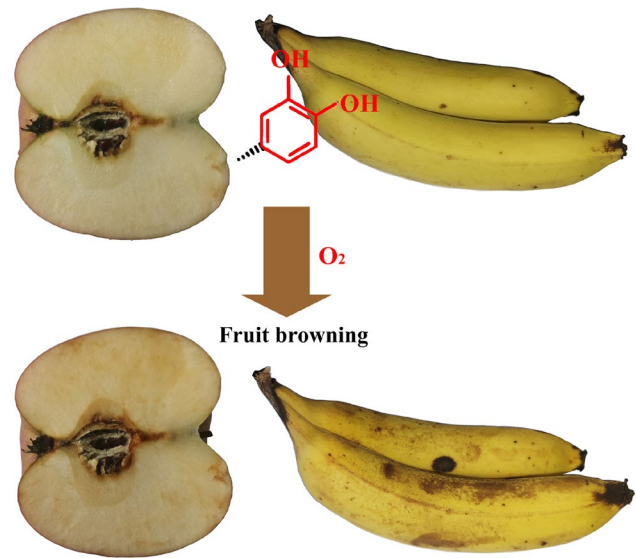


Fig. 1 Examples of spontaneous self-healing found in nature

plasma-sprayed coatings to further prolong the thermal cycling lifetime. Ouyang et al. introduced TiC as a self-healing agent into the YSZ coatings by APS, and found that the TiC-self-healing coatings improved the oxidation resistance and prolonged TBC lifetime [25, 26]. Portilla-Zea et al. reported the use of SiC microfibers as a self-healing agent in a TBC, and found that SiC-reinforced coating enhanced the adherence resistance and prolonged the cyclic oxidation time [27]. TiAl_3 intermetallic compounds showed excellent properties such as high melting point, low density, and good oxidation resistance at high temperatures [28]. Shen et al. reported that TiAl_3 showed the strong self-healing property, which could form an alumina protective layer in air at high temperatures [29]. However, the addition of TiAl_3 as a self-healing agent in YSZ TBCs has few reports.

In the present work, the double-layer TBCs of NiCrAlY/7YSZ were fabricated onto superalloy substrate. TiAl_3 particles with different fractions reinforced Ceria and Yttria-Stabilized Zirconia (CYSZ) ceramic were pre-placed on the as-sprayed TBCs and then post-treated by bionic laser alloying process. We investigated the influence of TiAl_3 content on the microstructure, phase composition, and thermal shock resistance of the bionic self-healing TBCs by fabricating the dotted bionic unit on its surface. Finally, the thermal shock failure mechanisms of bionic self-healing TBCs were elucidated.

2 Materials and Methods

2.1 Preparation of Bionic Self-healing TBCs

NiCrAlY powder (AMPERIT 413, H.C. Starck, Germany) was used for bond coating material. 7YSZ (ZrO_2 -7 wt.% Y_2O_3 , H.C. Starck, Germany) powder was used for top coating material. For the conventional TBCs, sand blasting was conducted before spraying and the NiCrAlY bond coating was deposited onto the K417G superalloy substrate buttons (having a diameter of 25.4 mm and a thickness of 6 mm) using a Low-Temperature High-Velocity Oxygen Fuel (LT-HVOF) spraying system (K2, GTV, Germany). And then, the 7YSZ top coating was sprayed on the bond coating by the APS system (MF-P 1000, GTV, Germany). The spraying parameters for NiCrAlY and 7YSZ were described in our previous study [22].

Figure 2 shows a schematic illustration of Bionic Laser Alloying (BLA). The $TiAl_3$ powder and CYSZ powder were used as raw materials. To obtain a homogeneous mixture, the powders were mixed in a ball grinding mill for 8 h. The ball-to-powder mass ratio was 30:1. The components of powder mixtures with different mass fractions are listed in Table 1. The mixed powders were pre-placed on the TBCs by a feeler gage before BLA. The thickness of pre-placed powder layer was approximately 0.1 mm. Bionic laser surface alloying experiments were performed by a pulsed Nd:YAG laser (XL-1000Y, China) with maximum laser power of 1000 W. The parameters of laser alloying process were listed as follows: laser power of 750 W, pulse duration of 5 ms, frequency of 1 Hz, and beam diameter of 1.5 mm. Based on the cylindrical substrate, bionic units are arranged in a circular pattern with unit distance of 3 mm.

Table 1 The components of powder mixtures

NO	$TiAl_3$ (wt.%)	CYSZ (wt.%)
BLA-1	5	95
BLA-2	15	85
BLA-3	25	75

2.2 Thermal Shock Test

Thermal shock test was performed by heating the as-sprayed and bionic self-healing coatings in an electric resistance furnace at 1000 °C for 5 min and then quenching in the deionized water. Subsequently, these coating specimens were taken out, and dried and put into the high-temperature furnace again to repeat the forementioned process. Once the spallation area reached to 20% of coating surface, the test was stopped and numbers of cycles were recorded to estimate the thermal shock resistance. The average thermal shock lifetimes of three specimens under the same condition were taken.

2.3 Coatings Characterization

The microstructures and fracture morphologies were investigated by a Scanning Electron Microscopy (SEM) fixed with Energy Dispersion Spectroscopy (EDS). The X-Ray Diffractometer (XRD) with filtered $Cu-K\alpha$ radiation was utilized to analyze phase composition. The scanning range was from 10° to 90° in 2θ with a scanning rate of 4° min^{-1} . Meanwhile, a slow scan at the 2θ range of 27°–33° and 72°–76° with a scanning rate of 0.2° min^{-1} was conducted.

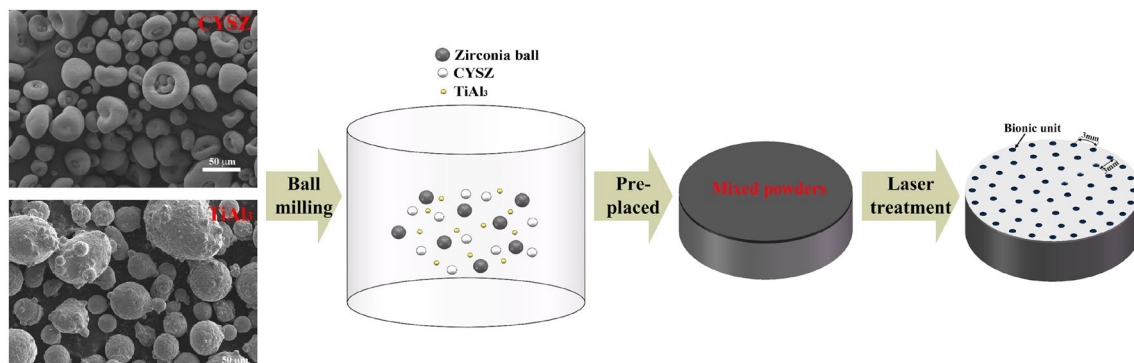


Fig. 2 Schematic illustration of TBCs processed by BLA

3 Results and Discussion

3.1 Microstructure

Figure 3 shows the surface morphologies of the as-sprayed and bionic self-healing coatings with different TiAl_3 fraction. It is obvious that the surface of the as-sprayed coating is coarse, which is covered by many pores, voids, and microcracks as depicted in Fig. 3a. After BLA treatment, the bionic self-healing coatings with different TiAl_3 fraction are obtained. For the bionic units with different TiAl_3 fraction, the surface of the bionic units is much smoother and filled with a few pores and some segmented microcracks. Noted that the number of segmented microcracks reduces with the TiAl_3 fraction increases, as shown in Fig. 3b, c and d. When the TiAl_3 fraction is 5%, the segmented microcracks are densely distributed on the bionic unit. When the TiAl_3 fraction is 25%, the number of segmented microcracks reduces significantly. It might be ascribed to the partial oxidation of TiAl_3 during laser treatment.

The cross-sectional morphologies of the as-sprayed and bionic self-healing TBCs with different TiAl_3 fraction are exhibited in Fig. 4. Obviously, the TBCs are composed of 7YSZ ceramic coating with a thickness of about $250 \pm 20 \mu\text{m}$ and NiCrAlY bond coating with a thickness of about $100 \pm 10 \mu\text{m}$, as shown in Fig. 4a. There are many pores, voids, and microcracks in the ceramic coating, which is the typical characteristic of air plasma

spraying. As for the bionic units with different TiAl_3 fraction, the microstructure of the bionic units is much denser shown in Fig. 4b, c, and d. Under the same condition of laser processing, the width of the bionic units with different TiAl_3 fraction is about 1.1 mm, and the depth of the bionic units ranges from $40 \mu\text{m}$ to $50 \mu\text{m}$. Similarly, when the TiAl_3 fraction is small, a few vertical microcracks can be observed in the bionic unit. However, when the TiAl_3 fraction is 25%, the vertical microcracks are not so clear.

Further observing the fracture morphologies of the as-sprayed and bionic self-healing TBCs with different TiAl_3 fraction (Fig. 5), it is obvious that the as-sprayed coating presents the lamellar structure (Fig. 5a), which is formed by the accumulating flattened splats during plasma spraying [30]. By contrast, when the TiAl_3 fraction is 5%, the fracture microstructure of the bionic unit is a coarse columnar crystal structure, as shown in Fig. 5b. However, when the TiAl_3 fraction is 15%, the columnar crystals are relatively small and there are many branched crystals along the growth direction (Fig. 5c). Furthermore, when the TiAl_3 fraction is 25%, the fracture microstructure of the bionic unit is a pseudo-columnar structure composed of closely linked partially melted particles (Fig. 5d), which was found in our previous studies [31] and other literature [32].

The microstructure evolution of the bionic unit prepared by BLA is mainly determined by temperature gradient (G) and solidification rate (R) at the front of the solid-liquid interface during the solidification process of the molten pool, namely constitutional supercooling formed by the difference between the temperature of the liquid and the actual

Fig. 3 Surface morphologies of **a** as-sprayed TBCs and bionic self-healing TBCs with **b** 5% TiAl_3 , **c** 15% TiAl_3 , and **d** 25% TiAl_3

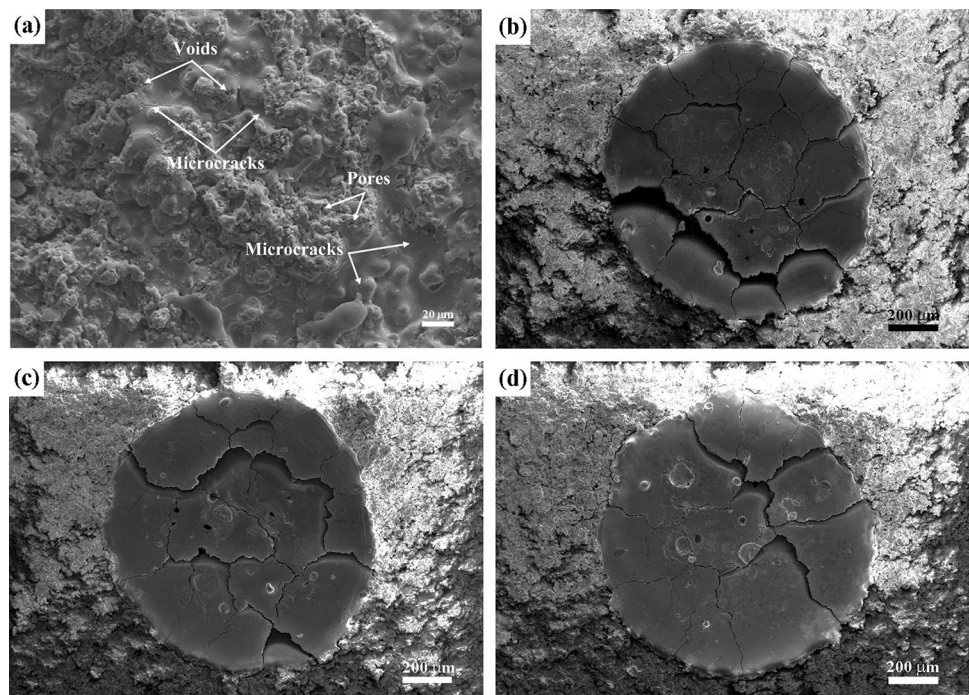


Fig. 4 Cross-sectional morphologies of **a** as-sprayed TBCs and bionic self-healing TBCs with **b** 5% TiAl_3 , **c** 15% TiAl_3 , and **d** 25% TiAl_3

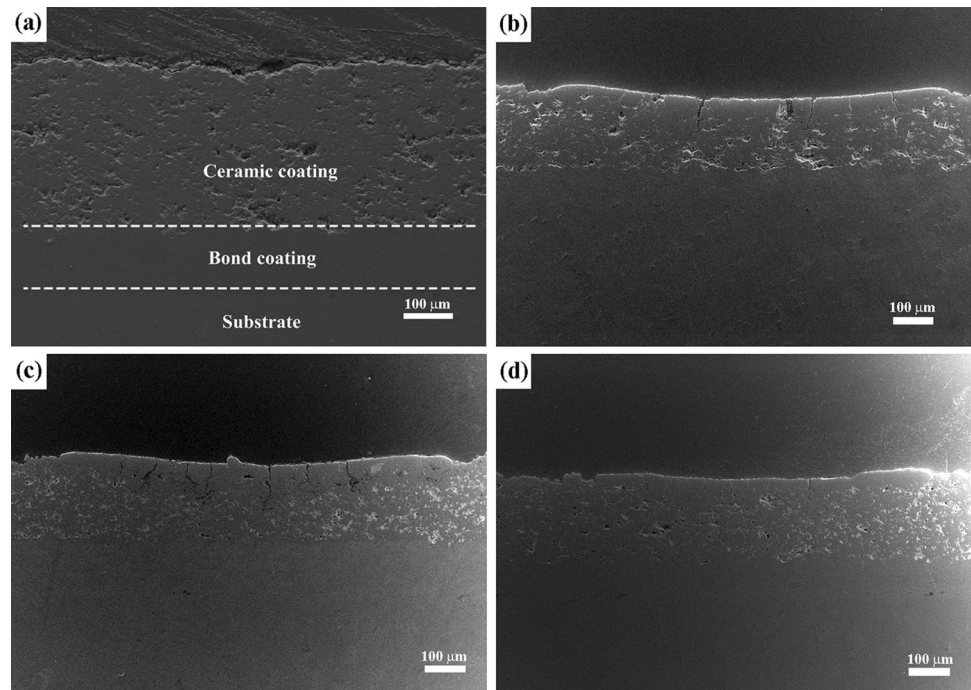
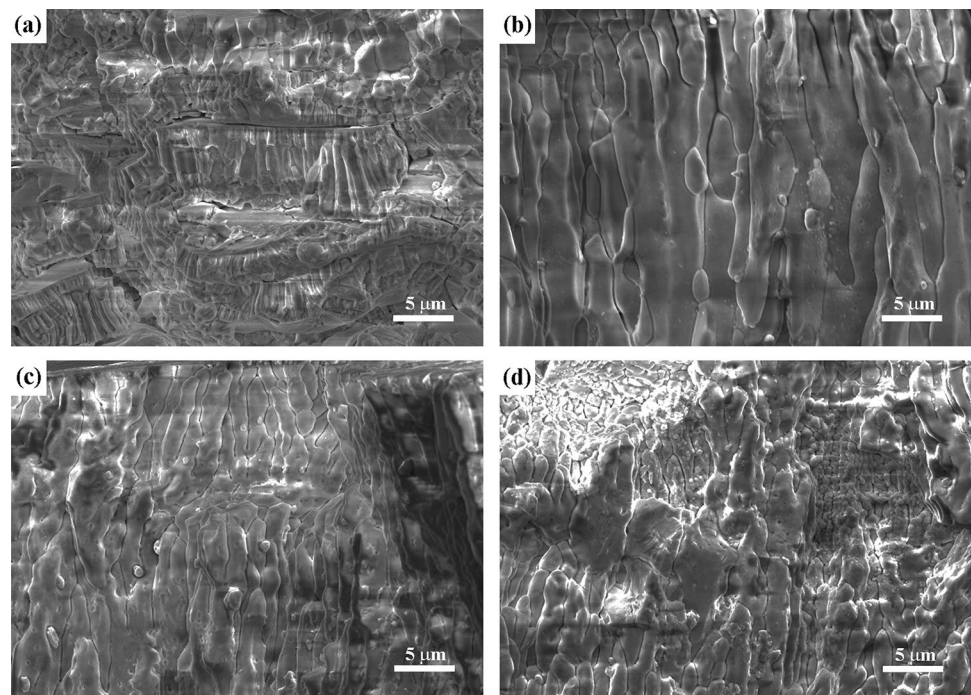


Fig. 5 Fracture morphologies of **a** as-sprayed TBCs and bionic self-healing TBCs with **b** 5% TiAl_3 , **c** 15% TiAl_3 , and **d** 25% TiAl_3



liquidus temperature at the front of the solid–liquid interface [33]. The ceramic coating is rapidly heated to form the molten pool under the action of laser irradiation. Due to the Gaussian distribution of the laser beam, a sharp thermal gradient forms between the center and the edge of the molten pool, leading to the formation of surface tension gradient and attendant Marangoni flow in the molten pool [34].

The original gas will escape from the molten pool under the stirring action of Marangoni flow, leading to the compact microstructure of bionic units. After the laser irradiation, the ratio of G and R at the interface between the 7YSZ ceramic layer and the bionic units is so high that the rapidly solidified microstructures of the bionic units are columnar crystals. Meanwhile, the rapid solidification of molten pool

during the BLA process results in the formation of vertical cracks, which are favorable for the strain tolerance capability of coating [35, 36]. As the fraction of TiAl_3 increases, the solute precipitated by the columnar crystal in the melts causes new constitutional supercooling, making the front of the columnar crystals unstable. Furthermore, new columnar crystals are formed at the side of the columnar crystals. Finally, these fine pseudo-columnar crystals are formed.

3.2 Phase Analysis

The XRD patterns of the as-sprayed and bionic self-healing TBCs with different TiAl_3 fraction are presented in Fig. 6. From Fig. 6a, it can be seen that the as-sprayed and bionic self-healing TBCs with different TiAl_3 fraction are all non-equilibrium tetragonal zirconia (t' - ZrO_2) and cubic zirconia (c - ZrO_2). Therefore, the BLA treatment has no effect on

the phase transformation of the as-sprayed 7YSZ ceramic. Further observing the XRD patterns of the as-sprayed and bionic self-healing TBCs at the 2θ range of 72° – 76° , it is found that diffraction peak intensity of t' - ZrO_2 becomes much larger after BLA treatment (Fig. 6b). However, for the bionic self-healing TBCs, diffraction peak intensity of t' - ZrO_2 gradually weakens with the TiAl_3 fraction increasing, which means the decrement of the beneficial t' - ZrO_2 .

3.3 Thermal Shock Behaviors

The macroscopic photographs of the as-sprayed TBCs and bionic self-healing TBCs with different TiAl_3 fraction during thermal shock test are shown in Fig. 7. For the as-sprayed and bionic self-healing TBCs with different TiAl_3 fraction, the spallation occurs at the edge and then extends to the neighboring zones. It can be seen from Fig. 7a that the initial

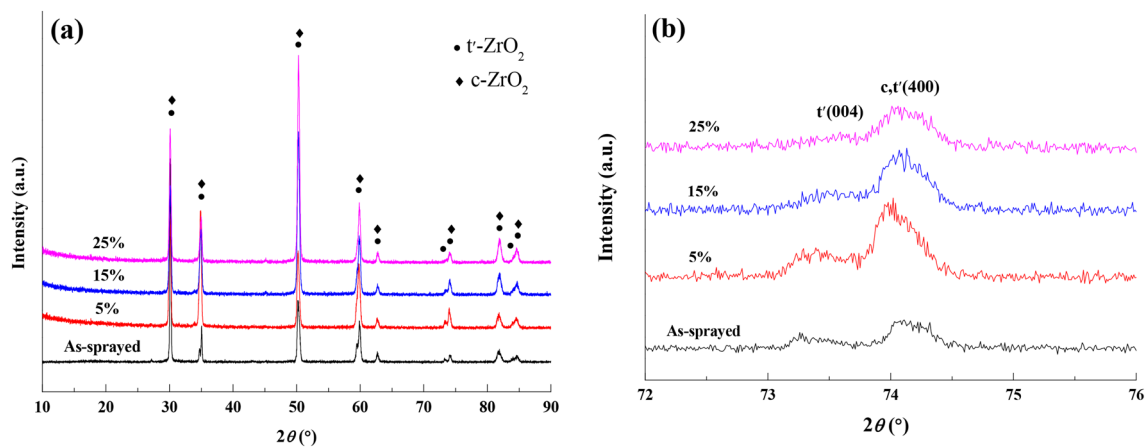


Fig. 6 The XRD patterns of the as-sprayed TBCs and bionic self-healing TBCs: **a** $2\theta = 20^\circ \sim 90^\circ$ and **b** $2\theta = 72^\circ \sim 76^\circ$

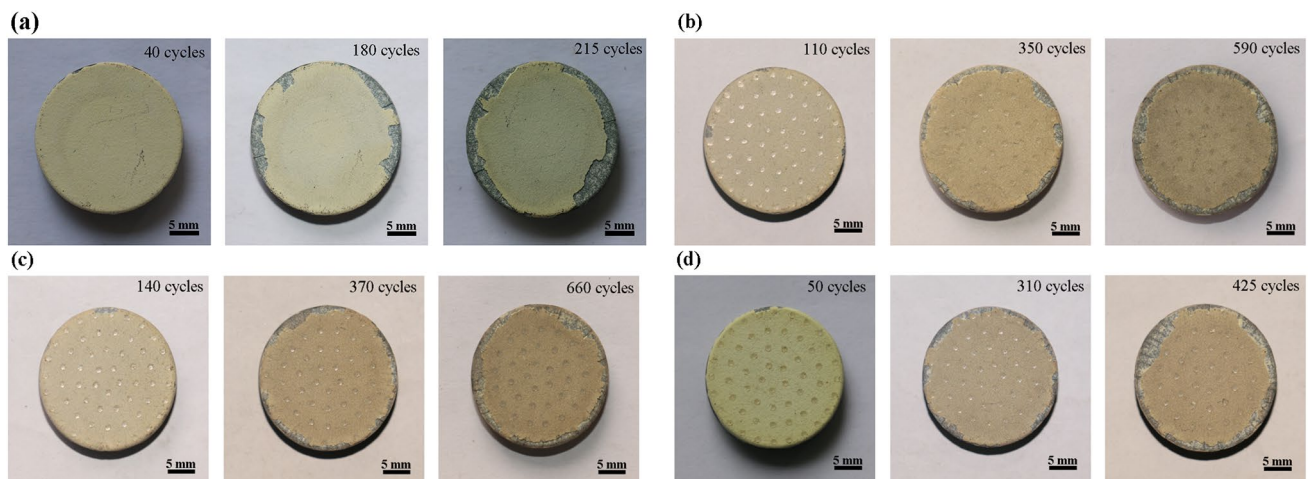


Fig. 7 Macro-photographs of **a** as-sprayed TBCs and bionic self-healing TBCs with different TiAl_3 fraction: **b** 5% TiAl_3 , **c** 15% TiAl_3 , and **d** 25% TiAl_3 during thermal shock tests

spallation thermal cycle of the as-sprayed coating is only 40, which is indicative of the early failure. Subsequently, the spallation ratio of the as-sprayed coating increases obviously; the spallation area ratio reaches 10% when the thermal shock cycle is 180. As the rapid heating and cooling cycle goes on, the as-sprayed specimen fails completely until 215 cycles. By contrast, the initial spallation thermal cycle of the bionic self-healing TBCs with 5%, 15% and 25% TiAl_3 is 110, 140, and 50, as shown in Fig. 7b, c, and d, respectively. This phenomenon indicates that the initial spallation of coatings can be postponed by the BLA treatment. Obviously, the spallation rate of the bionic self-healing TBCs is much slower than that of the as-sprayed TBCs. When the spallation area ratio reaches 10%, the corresponding thermal cycle of the bionic self-healing TBCs with 5%, 15%, and 25% TiAl_3 is 350, 370, and 310, respectively. It is worthy noted that the spallation of all bionic self-healing TBCs occurs between the outer edge and the bionic units. Eventually, the

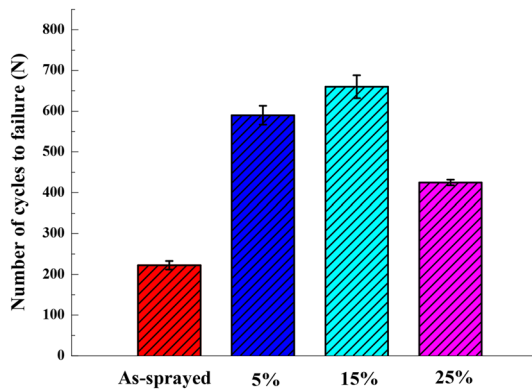


Fig. 8 The average thermal shock lifetimes of the as-sprayed and bionic self-healing TBCs with different TiAl_3 fraction

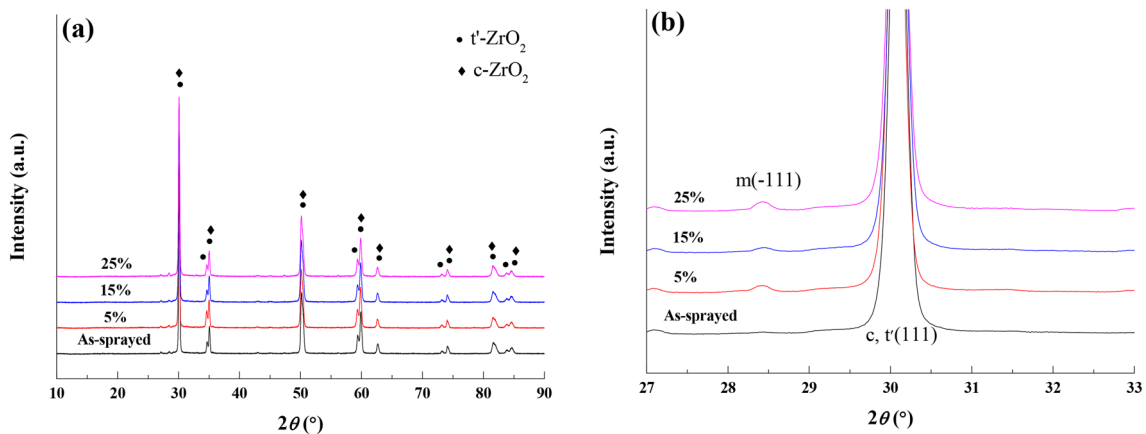


Fig. 9 The XRD patterns of the as-sprayed and bionic self-healing TBCs with different TiAl_3 fraction after thermal shock failure: **a** $2\theta = 10^\circ - 90^\circ$ and **b** $2\theta = 27^\circ - 33^\circ$

bionic self-healing TBCs with 5%, 15%, and 25% TiAl_3 fail after 590, 660, and 425 thermal cycles, respectively.

Figure 8 shows the average thermal shock lifetimes of the as-sprayed TBCs and bionic self-healing TBCs with different TiAl_3 fraction. It can be seen that the thermal shock resistance of all bionic self-healing TBCs is superior to that of the as-sprayed TBCs. This is mainly due to the segmented microcracks and columnar structure existed in the bionic self-healing TBCs, which is in favor of improving the strain tolerance of coatings [32, 37]. Among them, the bionic self-healing TBCs with 15% TiAl_3 show the best thermal shock resistance. The thermal shock lifetime of the bionic self-healing TBCs with 5%, 15%, and 25% TiAl_3 is 2.7 times, 3 times, and 1.9 times that of the as-sprayed TBCs, respectively. The excellent thermal shock resistance of the bionic self-healing TBCs is closely relevant to the microstructure of the bionic units. When the TiAl_3 fraction is 5%, columnar crystals are coarse and arranged orderly, which is beneficial to improve the strain tolerance of coating, enhancing the thermal shock resistance. When the TiAl_3 fraction is 15%, on one hand, the columnar crystals and vertical cracks could release the thermal stress during the thermal shock test; on the other hand, the oxidation products of TiAl_3 self-healing agent could seal the cracks during the high-temperature cycles, postponing the cracks connection. Therefore, the thermal shock resistance of the bionic self-healing TBCs with 15% TiAl_3 is the best. However, once the TiAl_3 fraction reaches 25%, these pseudo-columnar crystals with small structures and disordered growth directions are not conducive to the release of thermal stress during the thermal shock test, resulting in the decrement of thermal shock resistance.

The XRD patterns of the as-sprayed and bionic self-healing TBCs with different TiAl_3 fraction after thermal shock failure are depicted in Fig. 9. From Fig. 9a, it can be seen that the as-sprayed and bionic self-healing TBCs

with different TiAl_3 fraction are mainly composed of t' - ZrO_2 and c - ZrO_2 . In Fig. 9b, the diffraction peaks of m - ZrO_2 are not detected in the as-sprayed TBCs, while there is a small amount of detrimental m - ZrO_2 existed in the bionic self-healing TBCs with different TiAl_3 fraction. Since the as-sprayed TBCs failed completely after 215 thermal cycles, there is not enough heating time to transform t' - ZrO_2 into m - ZrO_2 . Thence, there is no harmful monoclinic m - ZrO_2 in the as-sprayed TBCs after thermal shock failure. By comparison, the bionic self-healing TBCs with different TiAl_3 fraction of 5%, 15%, and 25% have undergone long thermal cycles in the range of 425–660. Due to the long-term exposure to high temperature (1000 °C), t' - ZrO_2 phase decomposes into t - ZrO_2 phase and c - ZrO_2 phase. During cooling to room temperature, t - ZrO_2 phase might transform into m - ZrO_2 phase [38, 39]. The detrimental transformation of t - ZrO_2 to m - ZrO_2 accompanied by a significant volume expansion (3–5%) generally causes a high level of thermal stress [40], which might lead to the failure of the TBCs. However, the content of harmful m - ZrO_2 in the bionic self-healing TBCs with different TiAl_3 fraction is very small. Therefore, it can be said that the phase transformation is not the main reason for the thermal shock failure of the bionic self-healing TBCs.

Figure 10 shows the surface morphologies of the as-sprayed and bionic self-healing TBCs with different TiAl_3 fraction after thermal shock test. As for the as-sprayed TBCs, the surface becomes rougher and many tortuous microcracks are found after thermal shock test shown in Fig. 10a. As can be seen, there are still many pores and coarse segmented

microcracks on the surface of the bionic unit with a TiAl_3 fraction of 5%, as shown in Fig. 10b. It is obvious that the segmented microcracks on the surface of the bionic unit with a TiAl_3 fraction of 15% become much finer after thermal shock failure shown in Fig. 10c. When the TiAl_3 fraction is 25%, it is hard to see the segmented microcracks on the surface of the bionic unit after the thermal shock test (Fig. 10d). During the thermal shock test, TiAl_3 reacts with oxygen at high temperature. Then, the microcracks are gradually filled with the generated oxidation products, which realize the self-healing function of cracks. The more the content of TiAl_3 , the less the number of microcracks.

Figure 11 shows the high magnification surface morphologies of the as-sprayed and bionic self-healing TBCs with different TiAl_3 fraction after thermal shock test. From Fig. 11a, there are some pores on the surface of the as-sprayed TBCs and the coating spallation occurs around the tortuous microcracks. Meanwhile, it can be seen that the surface of the bionic units with different TiAl_3 fraction as well as the microcracks are covered with some white irregular particles after thermal shock test, as shown in Fig. 11b, c, and d.

Figure 12 exhibits the EDS analysis of the spots A, B, and C in Fig. 11. It can be found that there are O, Zr, Y, Ce, Ti, and Al elements in the white particle. The content of O and Zr elements is larger, the second is Al element, and Ti element content is the less, which indicates that oxidation reaction of TiAl_3 occurs during the thermal shock test. Smialek et al. studied the isothermal oxidation behavior of the cast TiAl_3 blocks and found that the oxidation product was

Fig. 10 Surface morphologies of TBCs after thermal shock test: **a** as-sprayed TBCs and bionic self-healing TBCs with **b** 5% TiAl_3 , **c** 15% TiAl_3 , and **d** 25% TiAl_3

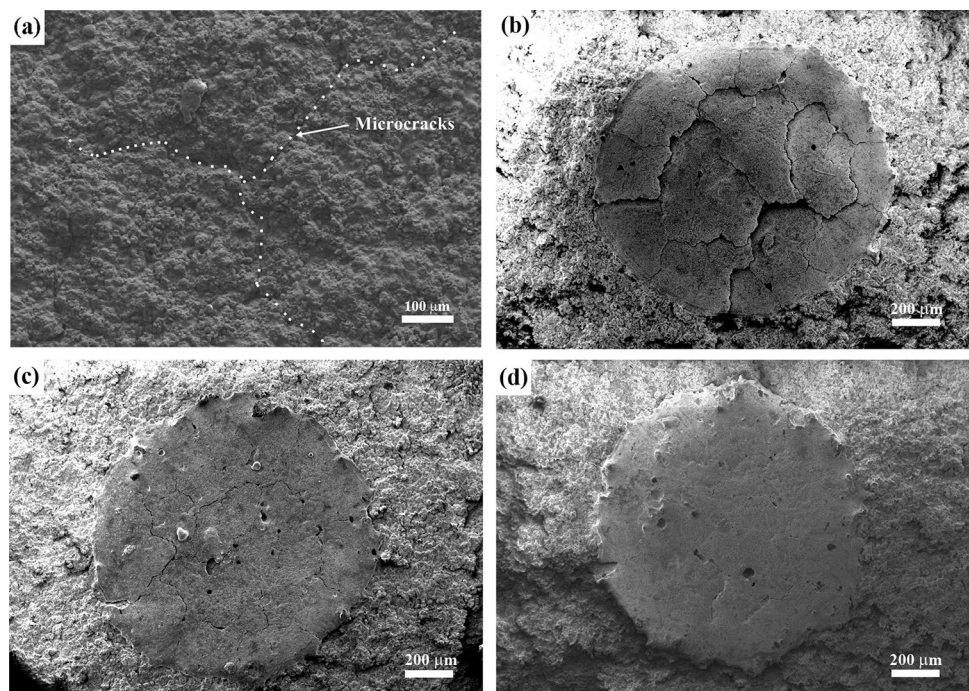


Fig. 11 High magnification surface morphologies of TBCs after thermal shock test: **a** as-sprayed TBCs and bionic self-healing TBCs with **b** 5% TiAl₃, **c** 15% TiAl₃, and **d** 25% TiAl₃

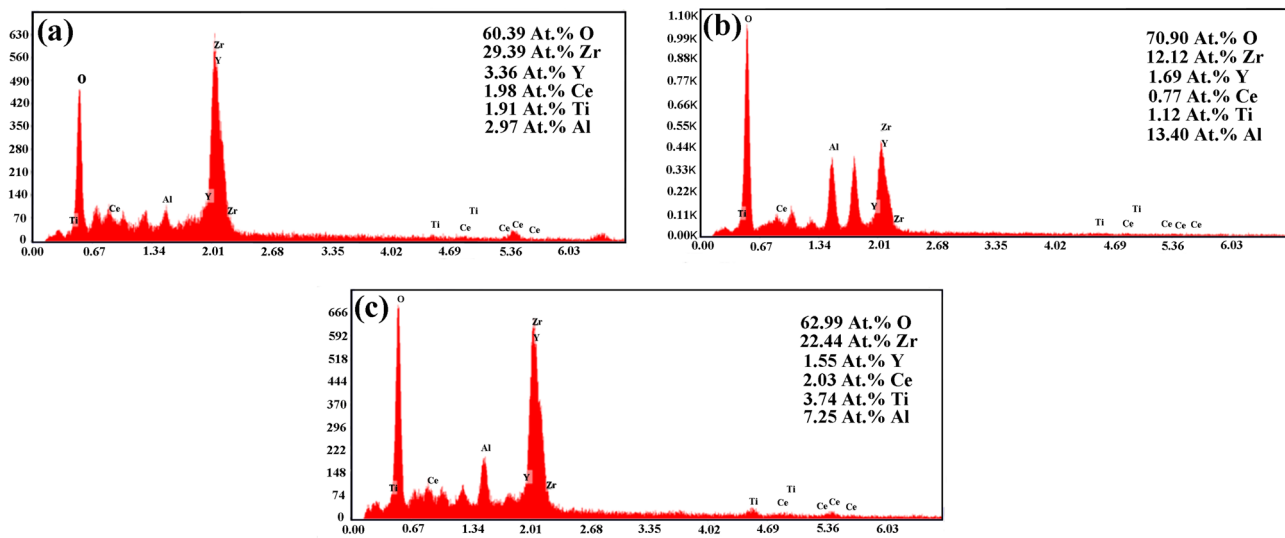
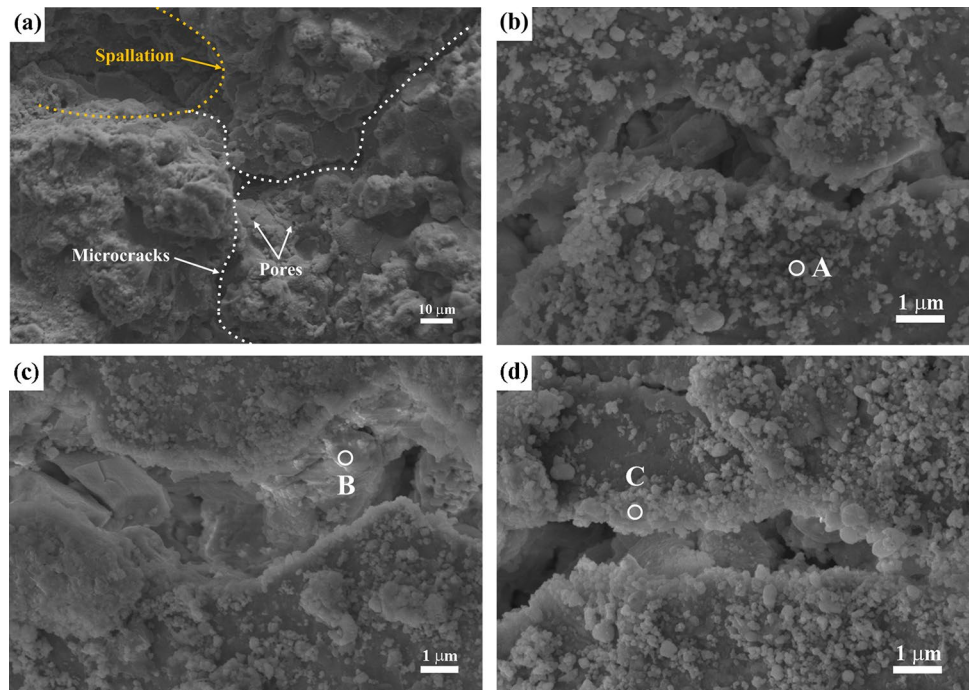
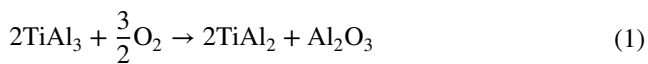


Fig. 12 EDS analysis of **a** spot A, **b** spot B, and **c** spot C in Fig. 11

only Al₂O₃ [41]. Chu et al. [42] fabricated a TiAl₃ film on the surface of Ti-50Al alloy and studied its high-temperature oxidation behavior at 1000 °C, they found that protective Al₂O₃ and TiAl₂ were formed on the outer surface, and TiO₂ was also found on the oxidized surface as the oxidation time prolonged. Therefore, the oxidation products of TiAl₃ in a long-term high-temperature oxidation environment are mainly Al₂O₃ and TiAl₂ as well as a small amount of TiO₂. According to the above XRD analysis in Fig. 9, TiAl₂, Al₂O₃, and TiO₂ phases were not detected in the

bionic self-healing TBCs with different TiAl₃ fraction after the thermal shock test. On one hand, because the amount of TiAl₃ is relatively small, the content of oxidation products is less; on the other hand, one limitation of XRD method makes it impossible to detect phases with low content.

Under high-temperature conditions, once the crack surface in the coating is in contact with oxygen in the atmosphere, the TiAl₃ in the bionic units will be oxidized to increase its volume. The oxidation reaction is as follows [43]:



under the long-term high-temperature conditions, TiAl₂ is further oxidized to Al₂O₃ and TiO₂ [43]. Due to the oxidation reaction of TiAl₃, the cracks are filled with the generated oxidation products. Therefore, the more TiAl₃ in the bionic units may lead to the obvious sealing effect. The volume expansion induced by the oxidation reaction can cause the filling or squeezing effect, and finally, the microcracks in the bionic units are healed. Theoretically, when the TiAl₃ particles are in direct contact with oxygen in the high-temperature atmosphere, the reaction speed is fast and the degree of reaction is relatively complete. Meanwhile, the TiAl₃ particles within the bionic units can also react with the permeable oxygen at the appropriate temperature and oxygen partial pressure, realizing the self-healing function of cracks. In this case, the reaction rate is slow and the degree of oxidation reaction is relatively incomplete.

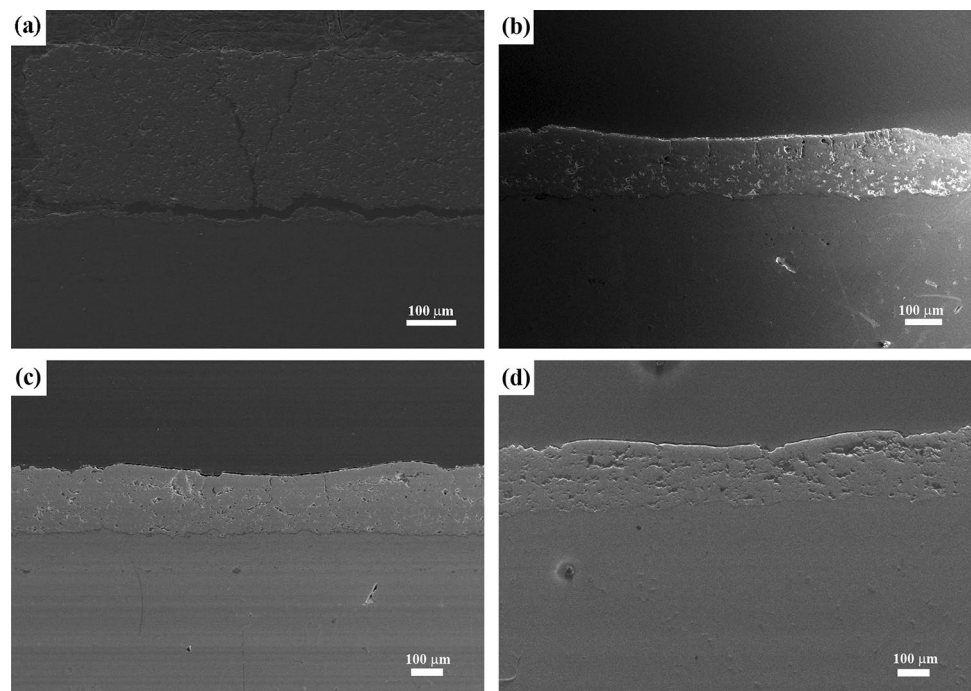
Figure 13 presents the cross-sectional morphologies of the as-sprayed and bionic self-healing TBCs with different TiAl₃ fraction after thermal shock test. From Fig. 13a, it is obvious that there is a serious delamination between the ceramic coating and the bond coating. Due to the oxygen penetration through the porous ceramic coating, the TGO layer is formed at the interface between the ceramic coating and the bond coating during the thermal shock test. The formed TGO layer could cause localized volume expansion, and the 7YSZ surrounding the TGO was subjected to additional tensile stress [19]. And it was found that the tensile

stress along the TC/TGO interface exhibited a continuously increasing trend with thermal cycling [44]. Thence, the transverse cracks are formed. Additionally, some vertical cracks are found in the as-sprayed ceramic coating after thermal shock test shown in Fig. 13a. The ceramic coating undergoes the serious high-temperature sintering during thermal cycling, accelerating the coating shrinkage and thermal expansion mismatch between the coating and the substrate. Furthermore, the thermal stress concentration will cause the crack initiation and crack propagation within the ceramic coating. As a result, the connection of transverse cracks and vertical cracks results in the eventual coating delamination and spallation.

As for the bionic self-healing TBCs with different TiAl₃ fraction, the number of microcracks in the bionic unit gradually decreases with the fraction of TiAl₃ increasing after the thermal shock test; that is, the microstructure of the bionic unit becomes denser. It can be seen from Fig. 13b that the number of vertical cracks in the bionic unit with 5% TiAl₃ after the thermal shock test is not significantly different from that before the thermal shock test. This is mainly because the low TiAl₃ content cannot trigger the crack healing mechanism. Compared with the bionic unit with 15% TiAl₃ before the thermal shock test (Fig. 4c), the vertical cracks are significantly reduced after the thermal shock test shown in Fig. 13c. When the TiAl₃ fraction is 25%, the bionic unit is almost completely dense after the thermal shock test shown in Fig. 13d.

Figure 14 shows the diagrammatic sketch of the thermal shock process in the bionic self-healing TBCs. The bionic laser

Fig. 13 Cross-sectional morphologies of TBCs after thermal shock test: **a** as-sprayed TBCs and bionic self-healing TBCs with **b** 5% TiAl₃, **c** 15% TiAl₃, and **d** 25% TiAl₃



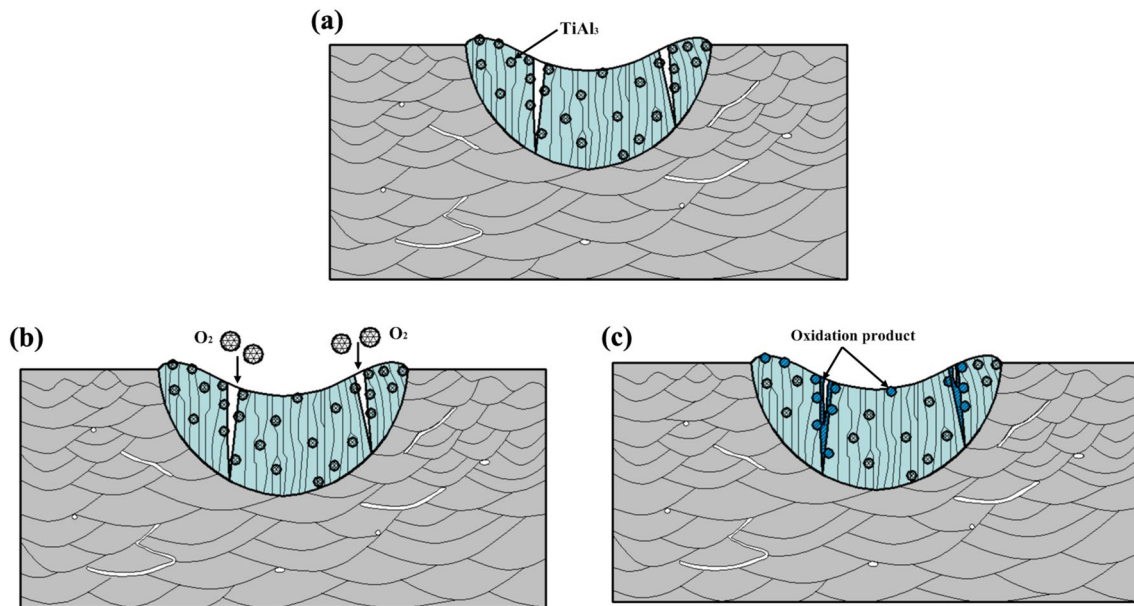


Fig. 14 Diagrammatic sketch of thermal shock process in the bionic self-healing TBCs: **a** the coating before thermal shock test, **b** early period of thermal shock test, and **c** later period of thermal shock test

alloying technology is utilized to melt the mixed powders of CYSZ ceramic and TiAl_3 intermetallic compound into the 7YSZ ceramic layer, thereby forming the bionic unit with vertical microcracks and a dense columnar crystal structure, and the TiAl_3 particles are randomly and uniformly distributed in the bionic unit, as shown in Fig. 14a. During thermal cycling at a high temperature of 1000 °C, the TiAl_3 on the surface of the bionic unit and around the vertical cracks will be in contact with oxygen in the atmosphere, as shown in Fig. 14b. Then, the self-healing agent TiAl_3 will react with oxygen to produce oxidation products, which can fill the microcracks and realize the partial self-healing of the microcracks, as depicted in Fig. 14c. During the early period of the thermal shock test, due to insufficient oxidation reaction, the vertical microcracks in the bionic units cannot be healed, and the columnar structure and vertical microcracks in the bionic self-healing TBCs can expand freely and release the thermal stress during the thermal shock test. During the later period of the thermal shock test, the healing of the vertical microcracks occurs with the oxidation time prolonging, and the connection between vertical microcracks and transverse microcracks are postponed. As a result, the thermal shock resistance of the bionic self-healing TBCs is improved enormously.

4 Conclusion

The microstructure, phase composition, and the thermal shock behaviors of the as-sprayed and the bionic self-healing TBCs with different TiAl_3 fraction were investigated. And several main conclusions can be drawn as follows:

- (1) The as-sprayed coating exhibited the typical lamellar structure consisting of pores, voids, and microcracks. After the BLA treatment, not only the microstructure was transformed from a porous lamella to a dense column or pseudo-column, but also the TiAl_3 self-healing agent was added into the bionic self-healing TBCs. The surface of the bionic self-healing TBCs was smooth and covered by segmented microcracks.
- (2) The thermal shock resistance of all bionic self-healing TBCs was much better than that of the as-sprayed TBCs. The bionic self-healing TBCs with 15% TiAl_3 had the best thermal shock resistance, whose thermal shock lifetime is three times that of the as-sprayed TBCs. On one hand, the columnar crystals and vertical cracks could improve strain compatibility of TBCs

during the thermal shock process; on the other hand, the oxidation reaction of TiAl₃ self-healing agent took place at high temperature to seal the microcracks, which could postpone the crack connection.

Acknowledgements This work is supported by National Natural Science Foundation of China (Grant No. 52105311), Natural Science Foundation of Zhejiang Province (Grant No. LQ21E010002), and Fundamental Research Funds for the Provincial Universities of Zhejiang (Grant No. RF-A2020009).

Declarations

Conflict of interests The authors have no relevant financial or non-financial interests to disclose.

References

- Tejero-Martin, D., Bai, M. W., Mata, J., & Hussain, T. (2021). Evolution of porosity in suspension thermal sprayed YSZ thermal barrier coatings through neutron scattering and image analysis techniques. *Journal of the European Ceramic Society*, *41*, 6035–6048.
- Kumar, N., Mahade, S., Ganvir, A., & Joshi, S. (2021). Understanding the influence of microstructure on hot corrosion and erosion behavior of suspension plasma sprayed thermal barrier coatings. *Surface and Coatings Technology*. <https://doi.org/10.1016/j.surfcoat.2021.127306>
- Reghu, V. R., Basha, A., Lobo, K., Shivakumar, S., Tilleti, P., Shankar, V., & Ramaswamy, P. (2019). Investigation on thermal barrier effects of 8YPSZ coatings on Al-Si alloy and validation through simulation. *Materials Today-Proceedings*, *19*, 630–636.
- Morelli, S., Testa, V., Bolelli, G., Ligabue, O., Molinari, E., Antolotti, N., & Lusvardi, L. (2020). CMAS corrosion of YSZ thermal barrier coatings obtained by different thermal spray processes. *Journal of the European Ceramic Society*, *40*, 4084–4100.
- Shi, M. C., Xue, Z. L., Zhang, Z. Y., Ji, X. J., Byon, E. S., & Zhang, S. H. (2020). Effect of spraying powder characteristics on mechanical and thermal shock properties of plasma-sprayed YSZ thermal barrier coating. *Surface and Coatings Technology*. <https://doi.org/10.1016/j.surfcoat.2020.125913>
- Zhang, P. P., Zhang, X. F., Li, F. H., Zhang, Z. H., Wang, Y. L., Li, H., Ren, L. Q., & Liu, M. (2019). Hot corrosion behavior of YSZ thermal barrier coatings modified by laser remelting and Al deposition. *Journal of Thermal Spray Technology*, *28*, 1225–1238.
- Ghadami, F., Aghdam, A. S. R., & Ghadami, S. (2020). Preparation, characterization and oxidation behavior of CeO₂-gradient NiCrAlY coatings applied by HVOF thermal spraying process. *Ceramics International*, *46*, 20500–20509.
- Slamecka, K., Jech, D., Klakurkova, L., Tkachenko, S., Remesova, M., Gejdos, P., & Celko, L. (2020). Thermal cycling damage in pre-oxidized plasma-sprayed MCrAlY plus YSZ thermal barrier coatings: Phenomenon of multiple parallel delamination of the TGO layer. *Surface and Coatings Technology*. <https://doi.org/10.1016/j.surfcoat.2019.125328>
- Chen, Y., Zhao, X. F., & Xiao, P. (2020). Effect of surface curvature on oxidation of a MCrAlY coating. *Corrosion Science*. <https://doi.org/10.1016/j.corsci.2019.108256>
- Chen, Y., Zhao, X. F., & Xiao, P. (2018). Effect of microstructure on early oxidation of MCrAlY coatings. *Acta Materialia*, *159*, 150–162.
- Soleimanipour, Z., Baghshahi, S., & Shoja-razavi, R. (2017). Improving the thermal shock resistance of thermal barrier coatings through formation of an in situ YSZ/Al₂O₃ composite via laser cladding. *Journal of Materials Engineering and Performance*, *26*, 1890–1899.
- Huang, Y. L., Shen, Y. T., Zeng, Y., Song, X. M., Lin, C. C., Zhang, J. M., & Guo, X. (2021). EBSD analysis of microstructure changes in YSZ coatings during thermal cycling. *Ceramics International*, *47*, 5559–5569.
- Nozahic, F., Monceau, D., & Estournes, C. (2016). Thermal cycling and reactivity of a MoSi₂/ZrO₂ composite designed for self-healing thermal barrier coatings. *Materials and Design*, *94*, 444–448.
- Ray, A. K., & Steinbrech, R. W. (1999). Crack propagation studies of thermal barrier coatings under bending. *Journal of the European Ceramic Society*, *19*, 2097–2109.
- Sun, J. Y., Tong, J., & Ma, Y. H. (2008). Nanomechanical behaviours of cuticle of three kinds of beetle. *Journal of Bionic Engineering*, *5*, 152–157.
- Lomakin, J., Arakane, Y., Kramer, K. J., Beeman, R. W., Kanost, M. R., & Gehrke, S. H. (2010). Mechanical properties of elytra from *Tribolium castaneum* wild-type and body color mutant strains. *Journal of Insect Physiology*, *56*, 1901–1906.
- Faisal, T. R., Abad, E. M. K., Hristozov, N., & Pasini, D. (2010). The impact of tissue morphology, cross-section and turgor pressure on the mechanical properties of the leaf petiole in plants. *Journal of Bionic Engineering*, *7*, S11–S23.
- Wang, X. S., Li, Y., & Shi, Y. F. (2008). Effects of sandwich microstructures on mechanical behaviors of dragonfly wing vein. *Composites Science and Technology*, *68*, 186–192.
- Song, J. R., Fan, C. C., Ma, H. S., Liang, L. H., & Wei, Y. G. (2018). Crack deflection occurs by constrained microcracking in nacre. *Acta Mechanica Sinica*, *34*, 143–150.
- Zhang, Z. H., Zhang, L., Yu, Z. L., Liu, J. J., Li, X. J., & Liang, Y. H. (2018). In-situ mechanical test of dragonfly wing veins and their crack arrest behavior. *Micron*, *110*, 67–72.
- Wu, L. S., Wang, T., Hu, Y., Liu, J. M., & Song, M. J. (2020). A method for improving the crack resistance of aluminum alloy aircraft skin inspired by plant leaf. *Theoretical and Applied Fracture Mechanics*. <https://doi.org/10.1016/j.tafmec.2019.102444>
- Zhang, P. P., Li, F. H., Zhang, X. F., Zhang, Z. H., Zhou, F. F., Ren, L. Q., & Liu, M. (2019). Thermal shock resistance of thermal barrier coatings with different surface shapes modified by laser remelting. *Journal of Thermal Spray Technology*, *28*, 417–432.
- Zhang, P. P., Sun, L., Zhang, X. F., Wang, Y. L., Zhang, Q. L., Yao, J. H., & Chang, F. (2021). Thermal cycling behavior of selective laser-remelted thermal barrier coatings with different laser dot distances. *Journal of Thermal Spray Technology*, *30*, 1038–1048.
- Wang, Y., Park, J. P., Hong, S. H., & Lee, H. (2016). Biologically inspired materials exhibiting repeatable regeneration with self-sealing capabilities without external stimuli or catalysts. *Advanced Materials*, *28*, 9961–9968.
- Ouyang, T. Y., & Suo, J. P. (2021). TiC-self-healing thermal barrier coating structures and oxidation resistance. *Surface and Coatings Technology*. <https://doi.org/10.1016/j.surfcoat.2021.127065>
- Ouyang, T. Y., Wu, J. Y., Yasir, M., Zhou, T., Fang, X. W., Wang, Y., Liu, D. W., & Suo, J. P. (2016). Effect of TiC self-healing coatings on the cyclic oxidation resistance and lifetime of thermal barrier coatings. *Journal of Alloys and Compounds*, *656*, 992–1003.
- Portilla-Zea, K., Gonzalez, M. A., Rodriguez, E., & Vasquez, G. I. (2021). Enhanced adhesion resistance of an 8YSZ thermal barrier coating through the formation of zircon and mullite as self-healing reaction products under cyclic oxidation conditions. *Materials Letters*. <https://doi.org/10.1016/j.matlet.2020.128697>
- Jiao, X. Y., Ren, X. R., Wang, X. H., Wang, S. G., Feng, P. Z., & Wang, J. Z. (2018). Porous TiAl₃ intermetallics with symmetrical

- graded pore-structure fabricated by leaching space holder and thermal explosion process. *Intermetallics*, 95, 144–149.
29. Shen, Z. J., Zhang, Y. N., Yu, X. H. (2019) Interfacial microstructure evolution mechanism of high temperature oxidation-resistant Al-based coating on Ti alloy surface. *Materials Research Express*, 6, 086472. <https://doi.org/10.1088/2053-1591/ab2a66>
 30. Wang, L., Zhong, X. H., Shao, F., Ni, J. X., Yang, J. S., Tao, S. Y., & Wang, Y. (2018). What is the suitable segmentation crack density for atmospheric plasma sprayed thick thermal barrier coatings with the improved thermal shock resistance? *Applied Surface Science*, 431, 101–111.
 31. Zhang, P. P., Zhang, X. F., Li, F. H., Zhang, Z. H., Li, H., Wang, Y. L., Ren, L. Q., & Liu, M. (2019). Effects of selective laser modification and Al deposition on the hot corrosion resistance of ceria and yttria-stabilized zirconia thermal barrier coatings. *Coatings*, 9, 353.
 32. Fan, Z. J., Wang, K. D., Dong, X., Duan, W. Q., Mei, X. S., Wang, W. J., Cui, J. L., & Lv, J. (2015). Influence of columnar grain microstructure on thermal shock resistance of laser re-melted ZrO₂-7 wt.% Y₂O₃ coatings and their failure mechanism. *Surface and Coatings Technology*, 277, 188–196.
 33. Wang, D. S., Tian, Z. J., Shen, L. D., Liu, Z. D., & Huang, Y. H. (2014). Effects of laser remelting on microstructure and solid particle erosion characteristics of ZrO₂-7wt%Y₂O₃ thermal barrier coating prepared by plasma spraying. *Ceramics International*, 40, 8791–8799.
 34. Zhang, Z. H., Zhou, H., Ren, L. Q., Tong, X., Shan, H. Y., & Li, X. Z. (2008). Surface morphology of laser tracks used for forming the non-smooth biomimetic unit of 3Cr2W8V steel under different processing parameters. *Applied Surface Science*, 254, 2548–2555.
 35. Dhineshkumar, S. R., Duraiselvam, M., Natarajan, S., Panwar, S. S., Jena, T., & Khan, M. A. (2016). Enhancement of strain tolerance of functionally graded LaTi₂Al₉O₁₉ thermal barrier coating through ultra-short pulse based laser texturing. *Surface and Coatings Technology*, 304, 263–271.
 36. Bai, Y., Han, Z. H., Li, H. Q., Xu, C., Xu, Y. L., Wang, Z., Ding, C. H., & Yang, J. F. (2011). High performance nanostructured ZrO₂ based thermal barrier coatings deposited by high efficiency supersonic plasma spraying. *Applied Surface Science*, 257, 7210–7216.
 37. Lee, J. H., Tsai, P. C., & Chang, C. L. (2008). Microstructure and thermal cyclic performance of laser-glazed plasma-sprayed ceria-yttria-stabilized zirconia thermal barrier coatings. *Surface and Coatings Technology*, 202, 5607–5612.
 38. Schulz, U. (2000). Phase transformation in EB-PVD yttria partially stabilized zirconia thermal barrier coatings during annealing. *Journal of the American Ceramic Society*, 83, 904–910.
 39. Liang, B., Ding, C. X., Liao, H. L., & Coddet, C. (2006). Phase composition and stability of nanostructured 4.7 wt.% yttria-stabilized zirconia coatings deposited by atmospheric plasma spraying. *Surface and Coatings Technology*, 200, 4549–4556.
 40. Witz, G., Shklover, V., Steurer, W., Bachegowda, S., & Bossmann, H. P. (2007). Phase evolution in yttria-stabilized zirconia thermal barrier coatings studied by rietveld refinement of X-ray powder diffraction patterns. *Journal of the American Ceramic Society*, 90, 2935–2940.
 41. Smialek, J. L., & Humphrey, D. L. (1992). Oxidation-kinetics of cast TiAl₃. *Scripta Metallurgica et Materialia*, 26, 1763–1768.
 42. Chu, M. S., & Wu, S. K. (2005). Oxidation behavior of Ti-50Al intermetallics with thin TiAl₃ film at 1000 degrees C. *Oxidation of Metals*, 63, 1–13.
 43. Gauthier, V., Dettenwanger, F., Schutze, M., Shemet, V., & Quadakkers, W. J. (2003). Oxidation-resistant aluminide coatings on gamma-TiAl. *Oxidation of Metals*, 59, 233–255.
 44. Wei, Z. Y., Cai, H. N., Tahir, A., Zhang, W. W., Li, X. F., Zhang, Y., Huang, Y. P., & Liu, Y. (2019). Stress states in plasma-sprayed thermal barrier coatings upon temperature cycling: Combined effects of creep, plastic deformation, and TGO growth. *Ceramics International*, 45, 19829–19844.

Publisher's Note Springer Nature remains neutral with regard to jurisdictional claims in published maps and institutional affiliations.